Unsteady Aerodynamic Gust Response Including Steady Flow Separation

Sanford Fleeter,* Vincent R. Capece,† and Hsiao-Wei D. Chiang‡
Purdue University, West Lafayette, Indiana

A series of experiments are performed to investigate and quantify the unsteady aerodynamic response of an airfoil to a high reduced frequency gust including the effects of the gust forcing function waveform, airfoil loading, and steady flow separation. This is accomplished by using an axial flow research compressor to experimentally model the high reduced frequency gust forcing function and replacing the last stage stator row with isolated instrumented airfoils. Appropriate data are correlated with predictions from flat plate and cambered airfoil convected gust models. The airfoil surface steady loading is shown to have a large effect on the unsteady aerodynamic response. Also, the steady flow separation has a significant influence on the gust response, particularly upstream of the separation point and in the airfoil trailing-edge region.

Nomenclature

C = airfoil chord
$\bar{C}_\ell$ = steady lift coefficient $\int_0^C (\bar{p}_p - \bar{p}_s)\, dx/\frac{1}{2}\rho U_t^2 C$
$\hat{C}_p$ = first harmonic unsteady pressure coefficient $\Delta\hat{p}/\rho V_x \hat{v}^+$
$\hat{C}_p$ = static pressure coefficient $(\bar{P} - \bar{P}_{\text{exit}})/\frac{1}{2}\rho U_t^2$
$\mathcal{K}$ = gust propagation direction vector
k_1 = reduced frequency, $\omega C/2V_x$
k_2 = transverse gust wave number
$\bar{p}$ = airfoil surface static pressure
$\bar{p}_{\text{exit}}$ = exit static pressure
$\Delta\hat{p}$ = first harmonic unsteady pressure difference
$\hat{u}^+$ = first harmonic chordwise gust
U_t = rotor blade tip speed
$\hat{v}^+$ = first harmonic transverse gust
V_x = absolute axial velocity
α_0 = angle of attack
ρ = inlet air density

Introduction

THE unsteady flow past a stationary airfoil is of primary concern in many important applications. For example, the unsteady interaction of an airfoil with gusts and similar vortical disturbances plays a significant role in the aerodynamics, dynamic loading, aeroelasticity, and acoustics of modern aircraft, missiles, helicopter rotors, advanced turboprops, and turbomachines. As a result, the interest in unsteady flow theory initiated by Theodorsen,[1] Kussner,[2] and Sears[3] has continued to the present.

Theoretical gust models have typically been restricted to thin-airfoil theory, with the unsteady gust disturbance assumed to be small as compared to the mean steady potential flowfield. However, in most applications, airfoils with arbitrary shape, large camber, and finite angles of attack are required. In an attempt to meet this need, Horlock[4] and Naumann and Yeh[5] developed heuristic second-order analyses that take into account some second-order terms. These analyses showed that the unsteady aerodynamic forces acting on an airfoil were affected by both the small incidence angle and the small airfoil camber. However, these models neglect some second-order terms and also assume a small angle of attack. Thus, these results are only approximate and cannot be extended to finite-incidence angles or large airfoil camber.

It is apparent that the thin airfoil approach is not adequate for many applications of interest. In this regard, Goldstein and Atassi[6] and Atassi[7] developed a theory for the inviscid incompressible flow past an airfoil that fully accounts for the distortion of the impinging gust by the mean flow. The theory assumes that the fluctuating flow velocity is small compared to the mean velocity, with the unsteady flow linearized about the full potential steady flow, and accounts for the effects of both airfoil profile and angle of attack.

Experimental investigations have typically been restricted to low-reduced-frequency aerodynamic gusts. In part, this is due to the difficulties associated with generating a periodic unsteady gust, with low reduced frequency gust tunnels having been developed by Holmes,[8] Satyanarayana, Gostelow, and Henderson,[9] and Ostdiek,[10] for example. Also contributing is the difficulty in obtaining and analyzing the fundamental high-frequency unsteady data that define both the aerodynamic forcing function and the resulting airfoil surface pressure distributions. The acquisition and analysis of such high-frequency data have only recently become possible with the development and availability of miniature high-response pressure transducers, digital instrumentation, and computers for both control of instrumentation and digital data acquisition and analysis.

The above noted experiments and analyses are all concerned with attached steady flow. Separated flow oscillating airfoil phenomena, including stall flutter and dynamic stall, also have been addressed. Thus, oscillating airfoil models and experiments have considered the effects of steady loading and flow separation, for example, Refs. 11–17. In this regard it should be noted that only minimal attention has been directed toward the effect of steady loading and flow separation on the unsteady aerodynamic response of an airfoil to a periodic gust.

In this paper the effects of the gust waveform, as characterized by the chordwise (parallel) and transverse (normal) gust

Received May 9, 1988; revision received Oct. 10, 1988.

*Professor, School of Mechanical Engineering and Director, Thermal Sciences and Propulsion Center. Associate Fellow AIAA.

†Air Force Research in Aero Propulsion Technology (AFRAPT) Trainee, Thermal Sciences and Propulsion Center, School of Mechanical Engineering.

‡Graduate Research Assistant, Thermal Sciences and Propulsion Center, School of Mechanical Engineering.

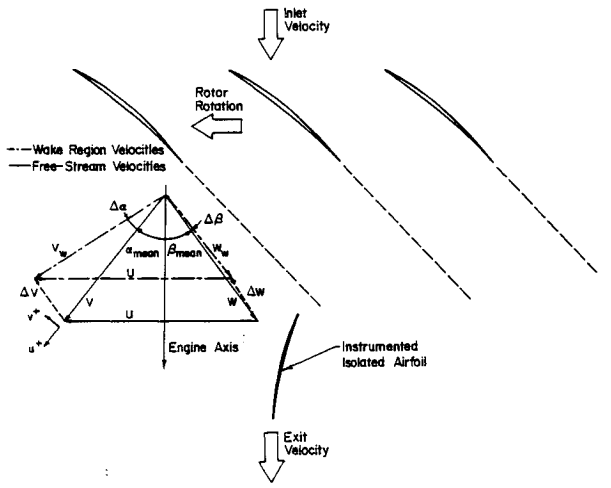

Fig. 1 Schematic of flowfield.

components u^+ and v^+ depicted in Fig. 1, airfoil loading, and steady flow separation on the unsteady aerodynamic response of an airfoil are experimentally investigated at high reduced frequency values for the first time. This is accomplished by 1) using an axial flow research compressor to experimentally model the high reduced frequency aerodynamic gust forcing function, 2) replacing the last stage stator row with instrumented isolated airfoils, and 3) developing and using computer-based time-variant digital data acquisition and analysis techniques, including ensemble averaging and Fast Fourier Transforms (FFT), for the analysis of the periodic data. In particular, high reduced frequency aerodynamic gusts are generated by the upstream rotor blade wakes, with the unsteady aerodynamic gust response determined by replacing the downstream stator row with static and dynamically instrumented isolated airfoils. Thus, there is complete experimental modeling of the basic unsteady aerodynamic phenomena inherent in this high reduced frequency unsteady interaction including angle-of-attack effects, the velocity and pressure variations, and the waveform of the aerodynamic forcing function.

Research Compressor

The Purdue axial flow research compressor with the last stage stator row replaced by an isolated airfoil is used for these experiments. It is driven by a 15 hP dc electric motor over a speed range of 300–3000 rpm. The wakes from the upstream rotor blades are the source of the unsteady surface pressures on the downstream isolated airfoil, i.e., the rotor wakes define the aerodynamic forcing function to the airfoil as depicted schematically in Fig. 1. The 43 rotor blades and the isolated airfoil are free vortex design airfoils with a British C4 section profile, a chord of 30 mm, and a maximum thickness-to-chord ratio of 0.10.

The variations in the airfoil steady loading are accomplished by compressor throttling and adjusting the setting angles of the instrumented airfoils, thereby altering the airfoil angle of attack. The detailed steady aerodynamic loading of the instrumented airfoils is specified by the chordwise distribution of the airfoil surface steady static pressure coefficient with the overall loading level given by the angle of attack and the steady lift coefficient.

The waveform of the aerodynamic forcing function is defined by the first harmonic chordwise and transverse gust components $\hat{u}^+$ and $\hat{v}^+$, respectively. The forcing function waveform variations to the instrumented last stage airfoils are accomplished by independently circumferentially indexing the upstream compressor vane rows relative to one another while maintaining a constant instrumented airfoil steady loading distribution.

Instrumentation

Both steady and unsteady data are required. The steady data define the detailed airfoil surface aerodynamic loading. The unsteady data quantify the time-variant aerodynamic forcing function to the isolated airfoil, i.e., the airfoil unsteady inlet flowfield and the resulting chordwise distribution of the time-variant pressures on the surfaces of the downstream airfoil. Flow visualization studies showed the flow to be two-dimensional on the midspan streamline. Thus, midspan chordwise distributions of airfoil surface static and dynamic instrumentation are used.

The unsteady aerodynamic forcing function to the airfoil, the time-variant inlet flowfield, is measured with a cross hot-wire probe. The airfoil mean absolute inlet flow angle is determined by rotating the cross-wire probe until a zero voltage difference is obtained between the two hot-wire signals. This mean angle is subsequently used as a reference to calculate the airfoil angle of attack and the instantaneous absolute and relative flow angles.

The airfoil surface time-variant pressure measurements are accomplished with flush-mounted ultraminiature high-response transducers. To minimize potential flow disturbances due to the transducer mounting or the inability of the transducer diaphragm to exactly maintain the surface curvature of the airfoil, a reverse mounting technique is used. The pressure surface of one airfoil and the suction surface of a second are instrumented, with the transducers embedded in the nonmeasurement surface and connected to the measurement surface by a static tap.

To assure the accuracy of the experiments and to minimize the number of stator row reconfigurations needed to obtain the isolated airfoil steady and unsteady data of interest, the complete last stage compressor stator row was replaced with a stator row comprised of only two airfoils, these being either the statically instrumented airfoils or the dynamically instrumented airfoils. This corresponds to a vane row with a solidity (chord/spacing) of less than 0.10, which results in a spacing between the instrumented vanes large enough so that the influence of the neighboring vanes is negligible, i.e., each vane is essentially an isolated airfoil. For example, the complex unsteady lift predicted by inviscid, incompressible transverse gust flat plate models at a reduced frequency of 5.0 are $(-0.0812, -0.1596)$ for an isolated airfoil and $(-0.0809, -0.1575)$ for a cascade with solidity of 0.1.

Data Acquisition and Analysis

The steady-state pressure data are acquired with a 48-channel Scanivalve system. Under computer control, the Scanivalve is calibrated each time data are acquired, with compensation automatically made for variations in the zero and span output. As part of the steady-state data acquisition and analysis process, a root mean square error analysis is performed. The steady data are defined as the mean of 30 samples, with the 95% confidence intervals determined.

The time-variant data from the hot-wire probe and the dynamic pressure transducers are obtained under computer control by first conditioning their signals and then digitizing them with a high-speed A-D system. This eight-channel system is able to digitize signals simultaneously at rates to 5 MHz per channel, storing 2048 points per channel. In addition, after conditioning the time-variant hot-wire and pressure transducer signals are monitored by a dynamic signal processor that can digitize, average, and Fourier decompose unsteady analog signals.

The time-variant data of interest are periodic, being generated at rotor blade passing frequency, with a digital ensemble averaging technique used for data analysis. As will be discussed, the key to this technique is the ability to sample data at a preset time. This is accomplished by means of an optical encoder mounted on the rotor shaft. The microsecond-range square wave voltage signal from the encoder is the time or data initiation reference that triggers the high-speed A-D

system. The time-variant signal is sampled and digitized over a time frame that is greater than the periodic signal component characteristic time. With the same initiation reference, i.e., the signal from the rotor-shaft-mounted optical encoder, a series of corresponding digitized signals is generated by repeating this signal sampling and digitization process. The time-variant signal ensemble average is then determined by averaging this series of digital data samples.

At each steady-state operating point, an averaged time-variant data set is obtained that consists of the hot-wire and the airfoil-mounted transducer signals digitized at a rate of 200 kHz and ensemble-averaged over 200 rotor revolutions. This sample rate allows approximately 91 points between each rotor blade at the design compressor rotational speed. These rotor revolutions are not consecutive due to the finite time required for the A-D multiplexer system to sample the data and the computer to then read the digitized data. Each of these digitized signals is Fourier decomposed into harmonics by means of a Fast Fourier Transform algorithm.

The first harmonic magnitude and phase angle referenced to the data initiation pulse are determined from the Fourier analysis of the data. To then relate the rotor-wake-generated velocity profiles with the first harmonic surface dynamic pressures on the instrumented downstream airfoil, the rotor exit velocity triangles are examined. The change in the rotor relative exit velocity that occurs as a result of the wake from a rotor blade is seen in Fig. 1. This velocity deficit creates a change in the absolute velocity vector, which is measured with the cross-wire probe. From this instantaneous absolute flow angle and velocity, the rotor exit relative flow angle and velocity and the amplitude and phase of the perturbation quantities are determined. The normal v^+ and parallel u^+ perturbation velocities are determined from the following relationships:

$$u^+ = V_{\text{mean}} - V_w \cos(\alpha - \alpha_{\text{mean}}), \qquad v^+ = V_w \sin(\alpha - \alpha_{\text{mean}}) \tag{1}$$

where V_{mean} is the mean flow velocity, V_w the wake velocity, α the wake absolute flow angle, and α_{mean} the mean absolute flow angle.

The hot-wire probe is positioned upstream of the leading edge of the instrumented airfoil. To relate time-based events as measured by this hot-wire probe to the unsteady pressures on the airfoil surfaces, the following assumptions are made: 1) the wakes are identical at the hot-wire and the instrumented airfoil leading-edge plane, and 2) the wakes are fixed in the relative frame. At a steady operating point, the hot-wire data are analyzed to determine the absolute flow angle and the rotor exit relative flow angle. Using the above two assumptions, the wake is located relative to the hot-wire and the leading edges of the instrumented airfoil suction and pressure surfaces. From this, the times at which the wakes are present at various locations are determined. The incremental times between occurrences at the hot-wire and the instrumented airfoil leading-edge plane are then related to phase differences between perturbation velocities and the airfoil surface.

The final form of the unsteady pressure data defines the chordwise variation of the first harmonic pressure difference across the chord-line of a stator vane and is presented as a nondimensional complex unsteady pressure difference across the airfoil chord in the format of the magnitude and the phase lag referenced to a transverse gust at the airfoil leading edge.

Predicted Gust Response

An unsteady aerodynamic gust response model that considers steady aerodynamic loading is needed to provide a baseline for accurate interpretation of the unsteady data. This is accomplished using the complete first-order model, i.e., the thin airfoil approximation is not used, and locally analytical solution developed by Chiang and Fleeter.[18] This model considers the flow of a two-dimensional unsteady aerodynamic gust convected with the mean flow past a thick, cambered airfoil at finite angle of attack α_0 as schematically depicted in Fig. 2. The periodic gust amplitude and harmonic frequency are denoted by A and ω, respectively. The two-dimensional gust propagates in the direction $\mathcal{K} = k_1\hat{\imath} + k_2\hat{\jmath}$, where k_1 is the reduced frequency, and k_2 is the transverse gust wave number, i.e., the transverse component of the gust propagation direction vector.

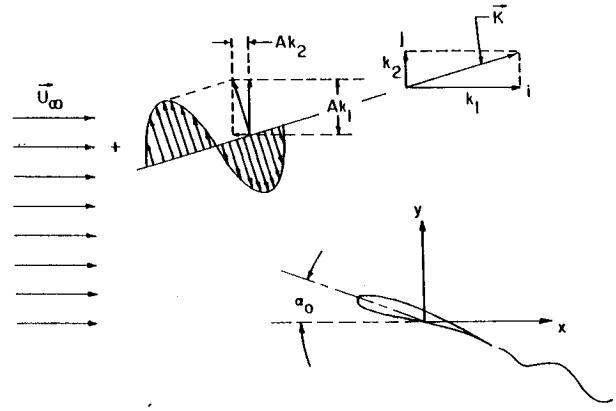

Fig. 2 Flow of a two-dimensional airfoil past a cambered airfoil.

The unsteady flowfield is considered to be rotational and is linearized about the full steady potential flow past the airfoil. Thus, the effects of airfoil thickness and camber as well as mean flow angle of attack are completely accounted for through the mean potential flowfield. The steady potential flowfield is independent of the unsteady flowfield. However, the strong dependence of the unsteady aerodynamics on the steady effects of airfoil geometry and angle of attack are manifested in the coupling of the unsteady and steady flowfields through the unsteady boundary conditions.

A locally analytical solution is then developed. In this method, the discrete algebraic equations that represent the flowfield equations are obtained from analytical solutions in individual grid elements. A body-fitted computational grid is used. General analytical solutions to the transformed Laplace equation are developed by applying these solutions to individual grid elements, i.e., the integration and separation constants are determined from the boundary conditions in each grid element. The complete flowfield is then obtained by assembling these locally analytical solutions.

Results

Nonseparated Flow

A low steady aerodynamic loading condition is established by setting the airfoil at an angle of attack of 0.1 deg. The data defining the airfoil surface static pressure distributions are presented in Fig. 3. There is a smooth chordwise pressure variation on each airfoil surface, with no indication of flow separation. Also, there is generally good correlation between the data and the inviscid Chiang-Fleeter cambered airfoil steady flow prediction, with the exception of the airfoil leading-edge region.

The aerodynamic gust waveform is characterized by the ratio of the first harmonic chordwise-to-normal gust components ($\hat{u}^+/\hat{v}^+$). The effect of the gust waveform on the unsteady aerodynamic response of the airfoil is considered by establishing compressor configurations such that the airfoil angle of attack and steady surface static pressure distributions are maintained per Fig. 3, but with the gust component ratio taking on values of 0.19, 0.35, and 0.53 (Fig. 4).

The effect of the aerodynamic gust waveform on the resulting unsteady pressure difference data is shown in Fig. 5. The

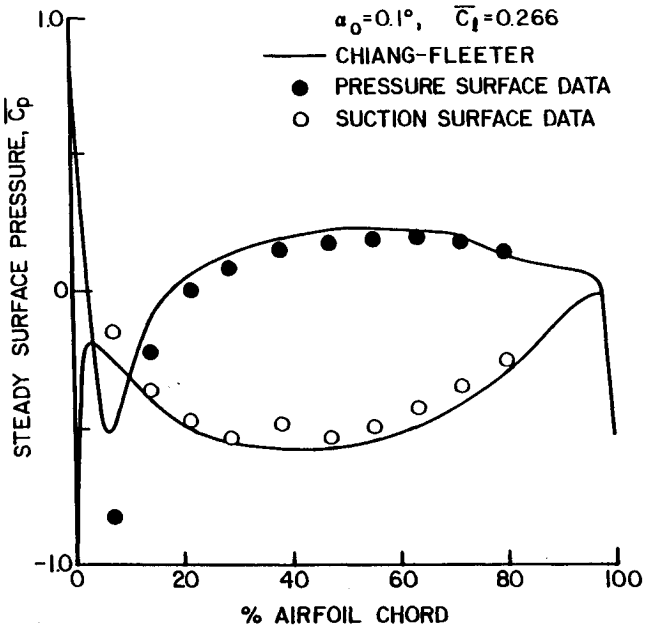

Fig. 3 Steady airfoil surface static pressure at low loading.

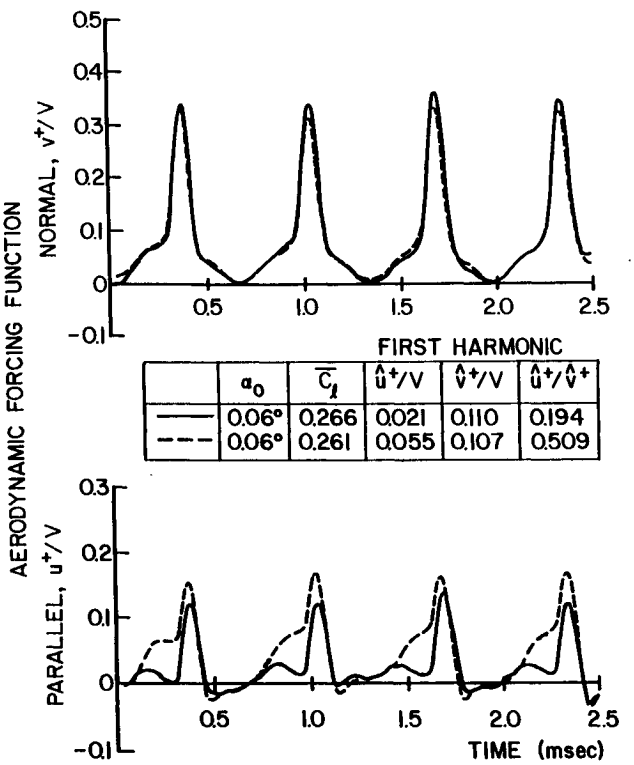

	α_0	$\bar{C}_l$	$\hat{u}^+/V$	$\hat{v}^+/V$	$\hat{u}^+/\hat{v}^+$
——	0.06°	0.266	0.021	0.110	0.194
- - -	0.06°	0.261	0.055	0.107	0.509

Fig. 4 Gust aerodynamic forcing functions at low loading.

profile of the airfoil and, thus, the surface steady loading distribution have a significant effect on the unsteady aerodynamic gust response. In particular, the chordwise variation of both the magnitude and the phase of the unsteady pressure difference generally exhibit much better correlation with the cambered airfoil predictions than with those from the flat plate model. The magnitude data exhibit good trendwise agreement with the cambered airfoil prediction, with this model typically overpredicting the magnitude of the pressure difference on the front 30% of the airfoil chord. This is due to the strong coupling of the unsteady prediction on an accurate representation of the steady flowfield. As previously noted, the steady flow prediction did not exhibit good correlation with the steady airfoil surface static pressure data over the front part of the airfoil. Hence, the poor unsteady data-prediction correlation in this region. Also, the ratio of the first harmonic gust components ($\hat{u}^+/\hat{v}^+$) has an effect on both the magnitude and phase of the unsteady pressure difference, although the general chordwise variation of these data is not affected.

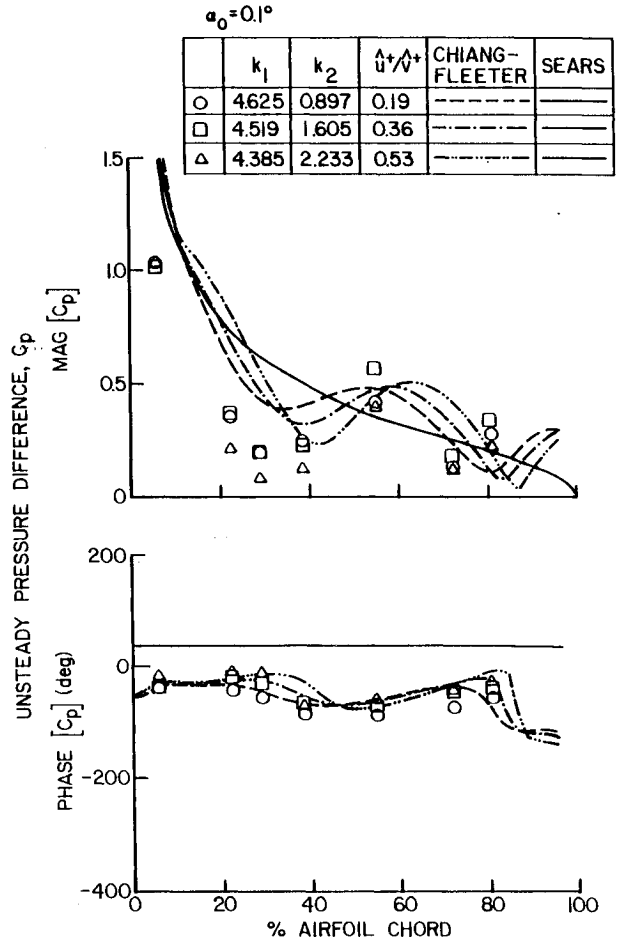

	k_1	k_2	$\hat{u}^+/\hat{v}^+$	CHIANG-FLEETER	SEARS
○	4.625	0.897	0.19	- - - - - -	——
□	4.519	1.605	0.36	- · - · - · -	——
△	4.385	2.233	0.53	- · · - · · -	——

Fig. 5 Effect of gust waveform on unsteady airfoil surface pressure difference at low loading.

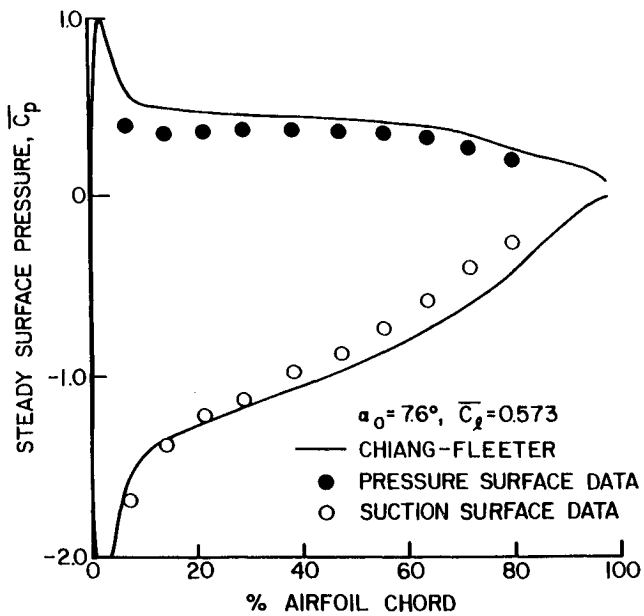

Fig. 6 Steady airfoil surface static pressure at intermediate loading.

To investigate the effect of steady airfoil loading on the aerodynamic gust response, the airfoil angle of attack was increased to 7.6 deg. The static pressure distributions on the airfoil suction and pressure surfaces together with the steady Chiang-Fleeter predictions are shown in Fig. 6. Relatively good correlation is obtained, although not quite as good as at the lower angle of attack. Again, the correlation between the data and the predictions is not very good in the leading-edge region of the airfoil.

The resulting unsteady aerodynamic gust response of the airfoil together with the flat plate and cambered airfoil predictions for a gust first-harmonic-component ratio of 0.22 are shown in Fig. 7. It should be noted that the reduced frequency k_1 for these intermediate angle-of-attack data is increased as compared to the previously presented low-angle-of-attack data. This is associated with the use of a low-speed research compressor to generate the aerodynamic gust forcing function. Again, the correlation of these complex unsteady pressure data with the cambered airfoil predictions is much better than with the flat plate model. In particular, the chordwise variations of both the magnitude and phase of the unsteady pressure-difference data exhibit good trendwise agreement with the cambered airfoil predictions. However, the phase correlation is not quite as good as at the lower loading level, with the magnitude data now overpredicted on the front half of the airfoil. This is again associated with the poor correlation between the steady surface pressure data and the model over the front part of the airfoil and the dependence of the unsteady predictions on the steady flow-field.

Figure 8 shows the correlation between the unsteady pressure-difference data and the corresponding predictions for 1) the Sears flat plate airfoil convected gust analysis, 2) the cambered airfoil convected gust model developed by Chiang and Fleeter, and 3) the cambered airfoil interaction gust model of Atassi. The magnitude data exhibit relatively good correlation with all three predictions, with consideration of the airfoil profile and steady loading resulting in the best correlation regardless of whether the gust is considered to be convected with the mean flow or not. The phase data correlate well with the cambered airfoil predictions and not the flat plate one, with the best correlation obtained with the convected gust cambered airfoil prediction. This is due to the coupling between the unsteady airfoil aerodynamics and the steady flowfield.

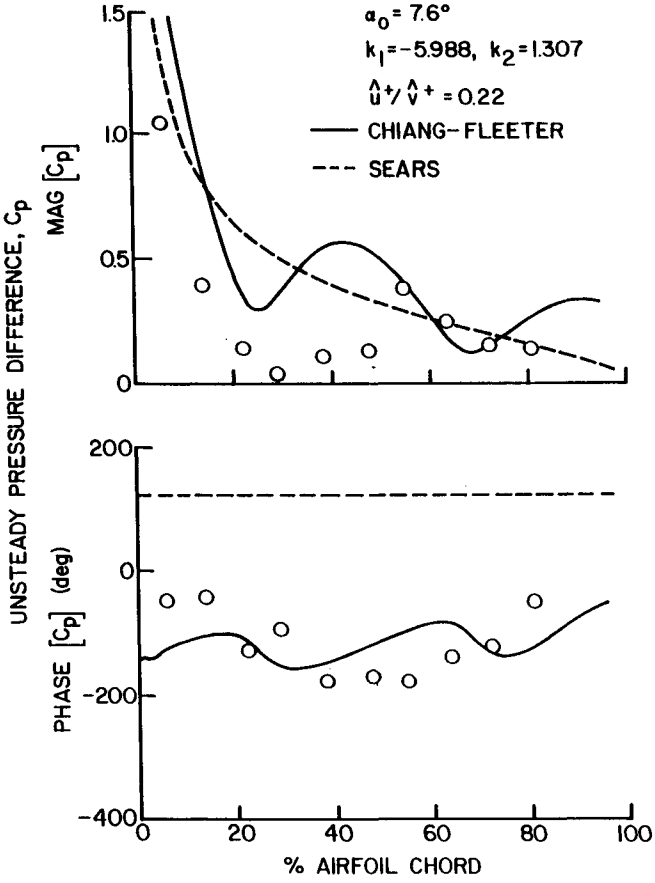

Fig. 7 Unsteady airfoil surface pressure differences at intermediate loading.

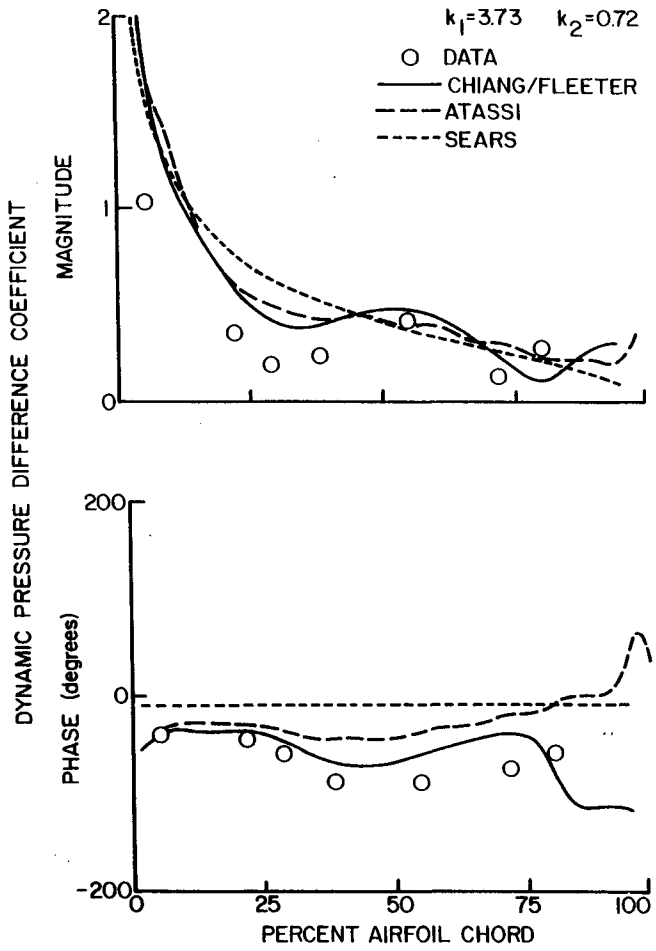

Fig. 8 Unsteady pressure difference correlation.

Separated Flow

Steady flow separation at approximately 35% of the airfoil suction surface was established by increasing the angle of attack to 14 deg. (Fig. 9). The effects of this flow separation on the unsteady aerodynamic gust response are investigated by comparing the resulting separated flow gust data with corresponding data obtained at the previous intermediate airfoil angle of attack of 7.6 deg. where the steady lift coefficient is nearly the same, but the steady flow is not separated. Also, both the parallel and normal gust components are maintained to be nearly identical for these two configurations (Fig. 10) with the ratio of the first-harmonic gust components being 0.218.

The resulting first-harmonic unsteady pressure difference data are presented in Fig. 11. Also shown is the nonseparated flat plate prediction of Sears. The cambered airfoil prediction is not presented because of the strong dependence of the cambered airfoil predictions on the steady flowfield and the inappropriateness of the inviscid steady model for separated flow. The magnitude data for the separated flow case show somewhat different trends than that for the nonseparated flow in the leading- and trailing-edge regions of the airfoil. For the separated flow configuration, the magnitude data are nearly

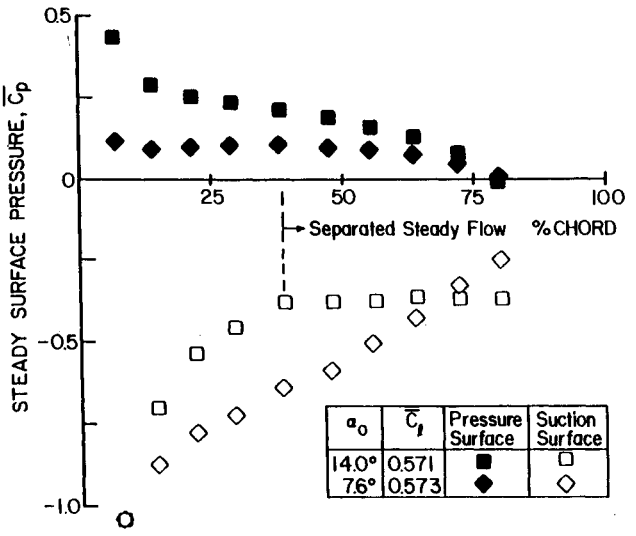

Fig. 9 Effect of suction surface flow separation on steady surface static pressure.

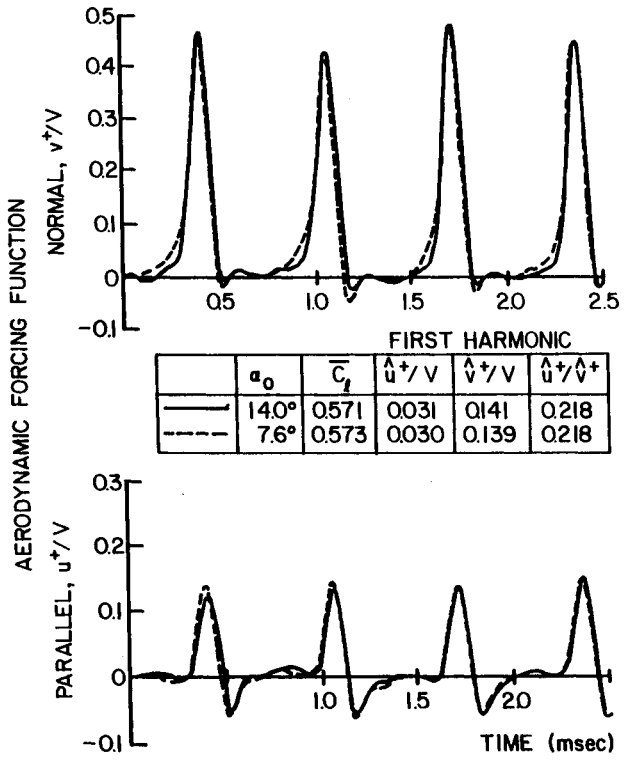

Fig. 10 Gust forcing functions for attached and separated flows.

constant over the front 15% of the airfoil, whereas the nonseparated data and the prediction indicate a decreasing amplitude. Aft of 15% chord, the magnitude data show analogous trends, with both the separated and nonseparated data decreasing with increasing chordwise position and attaining a minimum pressure amplitude value at 30% chord, similar to the previous results. The magnitude data for both cases then gradually increase to values that are greater than the prediction near midchord, with the nonseparated data being lower in amplitude up to this point due to the larger steady surface pressure differences between the suction and pressure surfaces. Both data sets then decrease with increasing chordwise position, with the separated data decreased in amplitude relative to the prediction and the nonseparated data. This is a result of the increased steady loading due to the separation in this region.

The phase data for the separated flow configuration have different trends than the nonseparated data and the flat plate prediction near the separation point and in the airfoil trailing-edge region. Over the front 20% of the airfoil, the data and the prediction show analogous trends of being nearly constant, with the separated data increased relative to the prediction and the nonseparated data. Aft of 20% chord, the separated phase data increase, whereas the nonseparated data decrease relative to the prediction. In the separated flow region, both the separated and nonseparated data show similar trends. However, at 70% chord the separated phase data jump to values larger than the prediction and increase with further chordwise position. On the other hand, the phase data for the nonseparated case show a gradual increase. Thus, separation affects both the magnitude and phase of the dynamic pressure difference data, with the primary effect being on the phase.

To further investigate these separation effects, individual suction surface time-variant pressure signals and their Fourier decompositions are considered. Figure 12 presents a typical unsteady pressure signal upstream of the separation point and the unsteady pressure signal at the same chordwise location for a configuration where the flow is not separated. It is clear that the downstream separation point affects both the amplitude and waveform of the unsteady pressure. This becomes more apparent in the spectrums of these nonseparated and separated unsteady pressures. The separated flow unsteady pressure has a much broader spectrum than the nonseparated one. This pressure field distortion is most probably due to the oscillation of the separation point generated by the periodic aerodynamic gusts. This would occur at the same frequency as the forcing function but would be out of phase with it.

A completely different trend is found within the separated flow region. Figure 13 presents the unsteady pressure signals for the separated and nonseparated flow cases for the same chordwise position and their resulting Fourier decomposition. There is little difference between the separated and nonseparated unsteady pressures. However, the nonseparated unsteady pressure has slightly more distortion, which results in

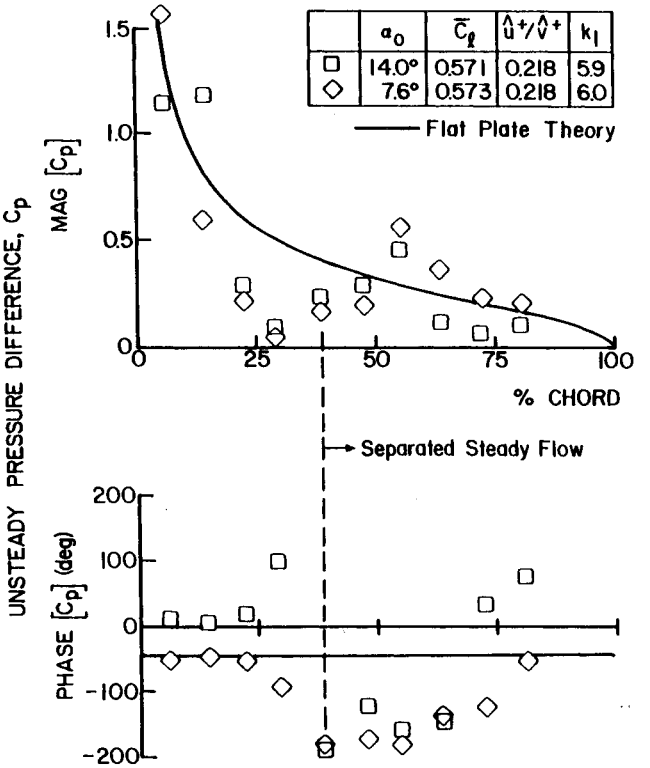

Fig. 11 Effect of suction surface flow separation on unsteady surface pressure.

the higher-order harmonics of the Fourier spectrum. This distortion is due to the steady flow turning and the aerodynamic loading of the airfoil. Within the separation zone where there is a constant steady static surface pressure, the pressure fluctuations generated by the separation-point oscillation are negligible, in contrast to the effect upstream of the separation point. Such a phenomenon also was noted by Maybey.[19] The effect of the separation-point oscillation is probably damped out by the mass of recirculating fluid within the separated flow region. Thus, the unsteady pressure within the separation zone is primarily responding to the aerodynamic forcing function.

The influence of the aerodynamic gust forcing function on the airfoil unsteady aerodynamics when the steady flow is separated is considered by establishing an additional airfoil configuration where the steady loading is nearly the same, having an angle of attack on the order of 14.0 deg., but the ratios of the gust components are different. The airfoil steady surface static pressure distributions for these two configurations are shown in Fig. 14. The airfoil pressure and suction surfaces have nearly identical distributions, with a fully separated flow starting at approximately 35% of the chord. Fig. 15 shows the areodynamic forcing function to the airfoil. The

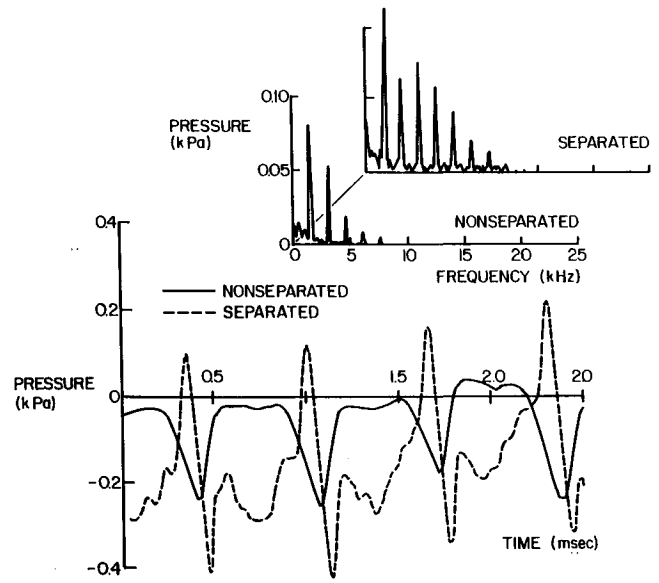

Fig. 12 Unsteady separated and attached flow pressure signals upstream of separation point.

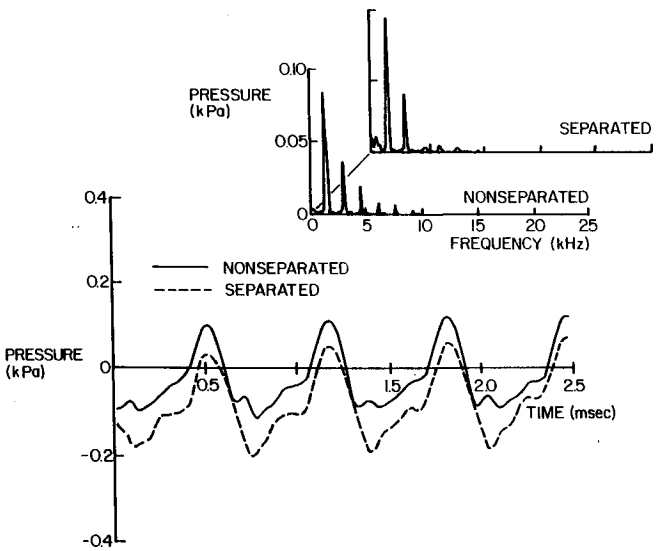

Fig. 13 Unsteady separated and attached flow pressure signals downstream of separation point.

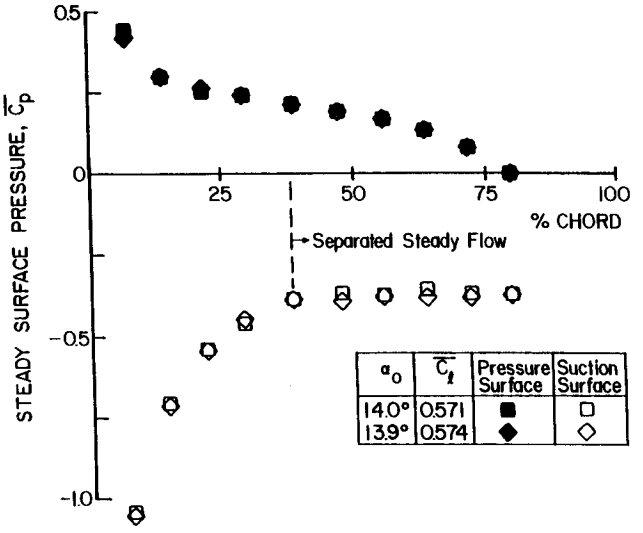

Fig. 14 Effect of gust waveform on airfoil surface steady static pressure.

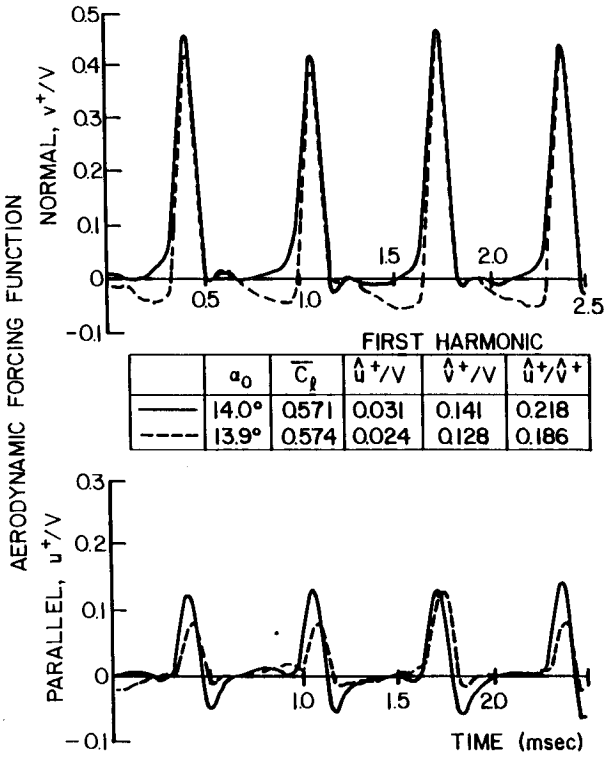

Fig. 15 Gust forcing function with suction surface flow separation.

first-harmonic ratios of the gust components ($\hat{u}^+/\hat{v}^+$) are 0.218 and 0.186, with both the normal $\hat{v}^+$ and the parallel $\hat{u}^+$ gust components having different values.

The first-harmonic unsteady pressure difference data for these two configurations, with the nonseparated flat plate prediction as a reference, are presented in Fig. 16. The magnitude data indicate analogous trends over the entire airfoil chord, with the 0.186 ($\hat{u}^+/\hat{v}^+$) data being decreased in value relative to both the prediction and the 0.218 ($\hat{u}^+/\hat{v}^+$) data. In the trailing-edge region, the data correlate well with each other and are decreased relative to the prediction due to the high steady loading in this region. The phase data show different trends than the previous high-loading cases and with each other near the separation point and the trailing edge. Over the front 25% of the chord, the phase data show the same trends, with the 0.186 ($\hat{u}^+/\hat{v}^+$) data being in closer agreement with the prediction. At 30% chord, the 0.218

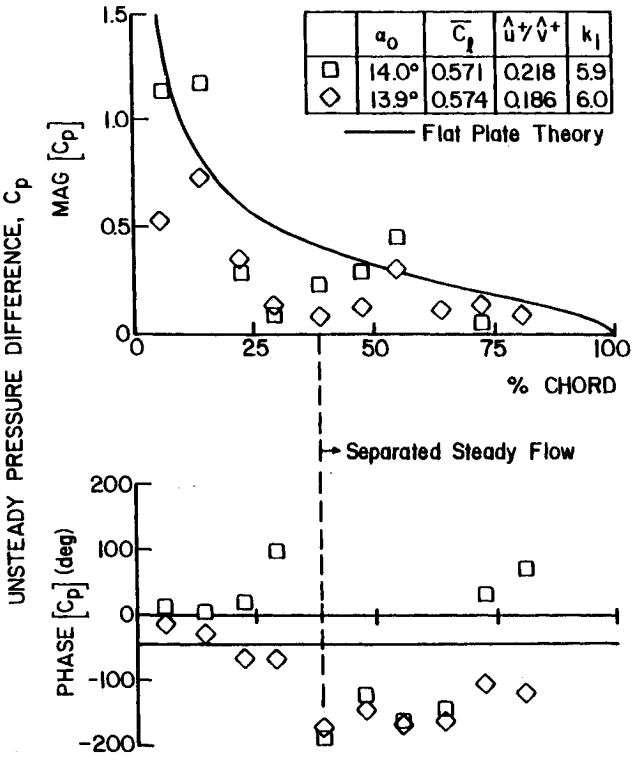

Fig. 16 Effect of gust waveform on unsteady pressure differences with separated steady flow.

($\hat{u}^+/\hat{v}^+$) data increase in phase, whereas the 0.186 ($\hat{u}^+/\hat{v}^+$) data continue to show good trendwise correlation with the prediction. From 40% to 60% chord, the phase data correlate with each other but are decreased in value with respect to the prediction. Aft of 60% chord, the 0.218 ($\hat{u}^+/\hat{v}^+$) phase data are increased relative to the prediction and increase with increasing chord. However, the phase data for 0.186 ($\hat{u}^+/\hat{v}^+$) first increase in phase and then indicate a slight decrease with increasing chordwise position.

Summary and Conclusions

A series of experiments have been performed to investigate and quantify the unsteady aerodynamic response of an airfoil to a high reduced frequency gust, including the effects of the gust-forcing-function waveform, airfoil steady loading, and steady flow separation. This was accomplished by using an axial flow research compressor to experimentally model the high reduced frequency gust-forcing function, with the last stage stator vane row replaced with isolated instrumented airfoils. Appropriate data were correlated with predictions from flat plate and cambered airfoil gust models.

At low and intermediate airfoil angles of attack with the steady flow not separated, the profile of the airfoil and, thus, the surface steady loading distribution were shown to have a significant effect on the unsteady aerodynamic gust response of the airfoil. Also, the ratio of the first harmonic gust components affects both the magnitude and phase of the unsteady pressure difference, although the general chordwise variation of these data was not affected. In addition, the magnitude data exhibit relatively good correlation with all three predictions, with consideration of the airfoil profile and steady loading resulting in the best correlation regardless of whether the gust is considered to be convected with the mean flow or not. The phase data correlate well with the cambered airfoil predictions and not the flat plate one, with the best correlation obtained with the convected gust cambered airfoil prediction. This is due to the coupling between the unsteady airfoil aerodynamics and the steady flowfield.

The steady flow separation was shown to have a significant influence on the unsteady aerodynamics on the airfoil surface upstream of the separation point and also in the trailing-edge region. Also, the separation affects both the magnitude and the phase of the unsteady pressure difference data, with the primary effect being on the phase. Consideration of the individual suction surface unsteady pressure signals revealed that 1) separation affects the magnitude, waveform, and spectrum of the unsteady pressure upstream of the separation point, possibly a result of an oscillation of the separation point due to the harmonic gust, 2) the pressure signals in the separated flow region and the corresponding signals with the flow not separated exhibit only small differences, and 3) there is a constant steady static surface pressure in the separated flow region.

Acknowledgment

Support of this experimental research program by the Air Force Office of Scientific Research, James Wilson, program manager, is gratefully acknowledged.

References

[1]Theodorsen, T., "General Theory of Aerodynamic Instability and the Mechanism of Flutter," NACA TR 496, 1935.

[2]Kussner, H. G., "Das Zweidimensionale Problem der Beliebig Bewgegten Tragflache unter Berucksichtigung von Patialbewegungen der Flussigkeit, *luftfahrtorsch*, Vol. 17, No. 355, 1940.

[3]Sears, W. R., "Some Aspects of Non-Stationary Airfoil Theory and its Practical Application," *Journal of the Aeronautical Sciences*, Vol. 104, No. 8, Jan. 1941, pp. 104–108.

[4]Horlock, J. H., "Fluctuating Lift Forces on Airfoils Moving Through Transverse and Chordwise Gusts," *ASME Journal of Basic Engineering*, Vol. 90, No. 4, Dec. 1968, pp. 494–500.

[5]Naumann, H., and Yeh, H., "Lift and Pressure Fluctuations of a Cambered Airfoil Under Periodic Gusts and Applications to Turbomachinery," *ASME Journal of Engineering for Power*, Vol. 95, No. 1, Jan. 1973, pp. 1–10.

[6]Goldstein, M. E., and Atassi, H., "A Complete Second-Order Theory for Unsteady Flow about an Airfoil due to a Periodic Gust," *Journal of Fluid Mechanics*, Vol. 74, 1976, pp. 741–765.

[7]Atassi, H. M., "The Sears Problem for a Lifting Airfoil Revisted-New Results," *Journal of Fluid Mechanics*, Vol. 141, 1984, pp. 109–122.

[8]Holmes, D. W., "Lift Measurements on an Airfoil in Unsteady Flow," American Society of Mechanical Engineers, New York, Paper 73-GT-41, 1973.

[9]Satyanarayana, B., Gostelow, J. P., and Henderson, R. E., "A Comparison Between Experimental and Theoretical Fluctuating Lift on Cascades at Low Frequency Parameters", American Society of Mechanical Engineers, New York, Paper 74-GT-78, 1974.

[10]Ostdiek, F. R., "A Cascade in Unsteady Flow," Air Force Aeropropulsion Lab. TR-76-115, Wright-Patterson AFB, Dec. 1976.

[11]Woods, L. C., "Aerodynamic Forces on an Oscillating Airfoil Fitted with a Spoiler," *Proceedings of the Royal Society of London*, Ser. A, No. 239, 1957. pp. 328–337.

[12]Yashima, S., and Tanaka, H., "Torsional Flutter in Stalled Cascade," American Society of Mechanical Engineers, New York, Paper 77-GT-72, 1977.

[13]Sisto, F., and Perumal, P. V. K., "Lift and Moment Predictions for an Oscillating Airfoil with a Moving Separation Point," *ASME Journal of Engineering for Power*, Vol. 96, No. 4, Oct. 1974, pp. 372–378.

[14]Ericsson, L. E., and Reding, J. P., "Unsteady Airfoil Stall, Review and Extension," *AIAA Journal*, Vol. 19, Aug. 1981.

[15]Carstens, V., "Theoretical Investigations on a Two-Dimensional Cascade in Incompressible Flow," Symposium on Unsteady Aerodynamics of Turbomachines and Propellers, Cambridge University Engineering, England, Sept. 1984, pp. 277–300.

[16]Chi, R. M., "Separated Flow Unsteady Aerodynamic Theory," *Journal of Aircraft*, Vol. 22, No. 11, Nov. 1985, pp. 956–964.

[17]Lorber, P. F., and Carta, F. D., "Airfoil Dynamic Stall at Constant Pitch Rate and High Reynolds Number," AIAA Paper 87-1329, 1987.

[18]Chiang, H. D., and Fleeter, S., "Prediction of Loaded Airfoil Unsteady Aerodynamic Gust Response by a Locally Analytical Method," *International Journal of Mathematical Modeling* (to be published).

[19]Maybey, D. G., "Analysis and Correlation of Data on Pressure Fluctuations in Separated Flow," *Journal of Aircraft*, Vol. 9, No. 9, Dec. 1972, pp. 642–645.